Measurement of the branching fraction and decay asymmetry of $\Lambda \to n\gamma$

M. Ablikim[1], M. N. Achasov[11,b], P. Adlarson[70], M. Albrecht[4], R. Aliberti[31], A. Amoroso[69A,69C], M. R. An[35], Q. An[66,53], X. H. Bai[61], Y. Bai[52], O. Bakina[32], R. Baldini Ferroli[26A], I. Balossino[27A], Y. Ban[42,g], V. Batozskaya[1,40], D. Becker[31], K. Begzsuren[29], N. Berger[31], M. Bertani[26A], D. Bettoni[27A], F. Bianchi[69A,69C], J. Bloms[63], A. Bortone[69A,69C], I. Boyko[32], R. A. Briere[5], A. Brueggemann[63], H. Cai[71], X. Cai[1,53], A. Calcaterra[26A], G. F. Cao[1,58], N. Cao[1,58], S. A. Cetin[57A], J. F. Chang[1,53], W. L. Chang[1,58], G. Chelkov[32,a], C. Chen[39], Chao Chen[50], G. Chen[1], H. S. Chen[1,58], M. L. Chen[1,53], S. J. Chen[38], S. M. Chen[56], T. Chen[1], X. R. Chen[28,58], X. T. Chen[1], Y. B. Chen[1,53], Z. J. Chen[23,h], W. S. Cheng[69C], S. K. Choi [50], X. Chu[39], G. Cibinetto[27A], F. Cossio[69C], J. J. Cui[45], H. L. Dai[1,53], J. P. Dai[73], A. Dbeyssi[17], R. E. de Boer[4], D. Dedovich[32], Z. Y. Deng[1], A. Denig[31], I. Denysenko[32], M. Destefanis[69A,69C], F. De Mori[69A,69C], Y. Ding[36], J. Dong[1,53], L. Y. Dong[1,58], M. Y. Dong[1,53,58], X. Dong[71], S. X. Du[75], P. Egorov[32,a], Y. L. Fan[71], J. Fang[1,53], S. S. Fang[1,58], W. X. Fang[1], Y. Fang[1], R. Farinelli[27A], L. Fava[69B,69C], F. Feldbauer[4], G. Felici[26A], C. Q. Feng[66,53], J. H. Feng[54], K Fischer[64], M. Fritsch[4], C. Fritzsch[63], C. D. Fu[1], H. Gao[58], Y. N. Gao[42,g], Yang Gao[66,53], S. Garbolino[69C], I. Garzia[27A,27B], P. T. Ge[71], Z. W. Ge[38], C. Geng[54], E. M. Gersabeck[62], A Gilman[64], K. Goetzen[12], L. Gong[36], W. X. Gong[1,53], W. Gradl[31], M. Greco[69A,69C], L. M. Gu[38], M. H. Gu[1,53], Y. T. Gu[14], C. Y Guan[1,58], A. Q. Guo[28,58], L. B. Guo[37], R. P. Guo[44], Y. P. Guo[10,f], A. Guskov[32,a], T. T. Han[45], W. Y. Han[35], X. Q. Hao[18], F. A. Harris[60], K. K. He[50], K. L. He[1,58], F. H. Heinsius[4], C. H. Heinz[31], Y. K. Heng[1,53,58], C. Herold[55], M. Himmelreich[31,d], G. Y. Hou[1,58], Y. R. Hou[58], Z. L. Hou[1], H. M. Hu[1,58], J. F. Hu[51,i], T. Hu[1,53,58], Y. Hu[1], G. S. Huang[66,53], K. X. Huang[54], L. Q. Huang[67], L. Q. Huang[28,58], X. T. Huang[45], Y. P. Huang[1], Z. Huang[42,g], T. Hussain[68], N Hüsken[25,31], W. Imoehl[25], M. Irshad[66,53], J. Jackson[25], S. Jaeger[4], S. Janchiv[29], E. Jang[50], J. H. Jeong[50], Q. Ji[1], Q. P. Ji[18], X. B. Ji[1,58], X. L. Ji[1,53], Y. Y. Ji[45], Z. K. Jia[66,53], H. B. Jiang[45], S. S. Jiang[35], X. S. Jiang[1,53,58], Y. Jiang[58], J. B. Jiao[45], Z. Jiao[21], S. Jin[38], Y. Jin[61], M. Q. Jing[1,58], T. Johansson[70], N. Kalantar-Nayestanaki[59], X. S. Kang[36], R. Kappert[59], M. Kavatsyuk[59], B. C. Ke[75], I. K. Keshk[4], A. Khoukaz[63], P. Kiese[31], R. Kiuchi[1], R. Kliemt[12], L. Koch[33], O. B. Kolcu[57A], B. Kopf[4], M. Kuemmel[4], M. Kuessner[4], A. Kupsc[40,70], W. Kühn[33], J. J. Lane[62], J. S. Lange[33], P. Larin[17], A. Lavania[24], L. Lavezzi[69A,69C], Z. H. Lei[66,53], H. Leithoff[31], M. Lellmann[31], T. Lenz[31], C. Li[39], C. Li[43], C. H. Li[35], Cheng Li[66,53], D. M. Li[75], F. Li[1,53], G. Li[1], H. Li[47], H. Li[66,53], H. B. Li[1,58], H. J. Li[18], H. N. Li[51,i], J. Q. Li[4], J. S. Li[54], J. W. Li[45], Ke Li[1], L. J Li[1], L. K. Li[1], Lei Li[3], M. H. Li[39], P. R. Li[34,j,k], S. X. Li[10], S. Y. Li[56], T. Li[45], W. D. Li[1,58], W. G. Li[1], X. H. Li[66,53], X. L. Li[45], Xiaoyu Li[1,58], H. Liang[66,53], H. Liang[30], H. Liang[1,58], Y. F. Liang[49], Y. T. Liang[28,58], G. R. Liao[13], L. Z. Liao[45], J. Libby[24], A. Limphirat[55], C. X. Lin[54], D. X. Lin[28,58], T. Lin[1], B. J. Liu[1], C. X. Liu[1], D. Liu[17,66], F. H. Liu[48], Fang Liu[1], Feng Liu[6], G. M. Liu[51,i], H. Liu[34,j,k], H. B. Liu[14], H. M. Liu[1,58], Huanhuan Liu[1], Huihui Liu[19], J. B. Liu[66,53], J. L. Liu[67], J. Y. Liu[1,58], K. Liu[1], K. Y. Liu[36], Ke Liu[20], L. Liu[66,53], Lu Liu[39], M. H. Liu[10,f], P. L. Liu[1], Q. Liu[58], S. B. Liu[66,53], T. Liu[10,f], W. K. Liu[39], W. M. Liu[66,53], X. Liu[34,j,k], Y. Liu[34,j,k], Y. B. Liu[39], Z. A. Liu[1,53,58], Z. Q. Liu[45], X. C. Lou[1,53,58], F. X. Lu[54], H. J. Lu[21], J. G. Lu[1,53], X. L. Lu[1], Y. Lu[7], Y. P. Lu[1,53], Z. H. Lu[1], C. L. Luo[37], M. X. Luo[74], T. Luo[10,f], X. L. Luo[1,53], X. R. Lyu[58], Y. F. Lyu[39], F. C. Ma[36], H. L. Ma[1], L. L. Ma[45], M. M. Ma[1,58], Q. M. Ma[1], R. Q. Ma[1,58], R. T. Ma[58], X. Y. Ma[1,53], Y. Ma[42,g], F. E. Maas[17], M. Maggiora[69A,69C], S. Maldaner[4], S. Malde[64], Q. A. Malik[68], A. Mangoni[26B], Y. J. Mao[42,g], Z. P. Mao[1], S. Marcello[69A,69C], Z. X. Meng[61], J. Messchendorp[12,59], G. Mezzadri[27A], H. Miao[1], T. J. Min[38], R. E. Mitchell[25], X. H. Mo[1,53,58], N. Yu. Muchnoi[11,b], Y. Nefedov[32], F. Nerling[17,d], I. B. Nikolaev[11,b], Z. Ning[1,53], S. Nisar[9,l], Y. Niu [45], S. L. Olsen[58], Q. Ouyang[1,53,58], S. Pacetti[26B,26C], X. Pan[10,f], Y. Pan[52], A. Pathak[30], M. Pelizaeus[4], H. P. Peng[66,53], K. Peters[12,d], J. L. Ping[37], R. G. Ping[1,58], S. Plura[31], S. Pogodin[32], V. Prasad[66,53], F. Z. Qi[1], H. Qi[66,53], H. R. Qi[56], M. Qi[38], T. Y. Qi[10,f], S. Qian[1,53], W. B. Qian[58], Z. Qian[54], C. F. Qiao[58], J. J. Qin[67], L. Q. Qin[13], X. P. Qin[10,f], X. S. Qin[45], Z. H. Qin[1,53], J. F. Qiu[1], S. Q. Qu[56], S. Q. Qu[39], K. H. Rashid[68], C. F. Redmer[31], K. J. Ren[35], A. Rivetti[69C], V. Rodin[59], M. Rolo[69C], G. Rong[1,58], Ch. Rosner[17], S. N. Ruan[39], H. S. Sang[66], A. Sarantsev[32,c], Y. Schelhaas[31], C. Schnier[4], K. Schoenning[70], M. Scodeggio[27A,27B], K. Y. Shan[10,f], W. Shan[22], X. Y. Shan[66,53], J. F. Shangguan[50], L. G. Shao[1,58], M. Shao[66,53], C. P. Shen[10,f], H. F. Shen[1,58], X. Y. Shen[1,58], B. A. Shi[58], H. C. Shi[66,53], J. Y. Shi[1], q. q. Shi[50], R. S. Shi[1,58], X. Shi[1,53], X. D Shi[66,53], J. J. Song[18], W. M. Song[30,1], Y. X. Song[42,g], S. Sosio[69A,69C], S. Spataro[69A,69C], F. Stieler[31], K. X. Su[71], P. P. Su[50], Y. J. Su[58], G. X. Sun[1], H. Sun[58], H. K. Sun[1], J. F. Sun[18], L. Sun[71], S. S. Sun[1,58], T. Sun[1,58], W. Y. Sun[30], X Sun[23,h], Y. J. Sun[66,53], Y. Z. Sun[1], Z. T. Sun[45], Y. H. Tan[71], Y. X. Tan[66,53], C. J. Tang[49], G. Y. Tang[1], J. Tang[54], L. Y Tao[67], Q. T. Tao[23,h], M. Tat[64], J. X. Teng[66,53], V. Thoren[70], W. H. Tian[47], Y. Tian[28,58], I. Uman[57B], B. Wang[1], B. L. Wang[58], C. W. Wang[38], D. Y. Wang[42,g], F. Wang[67], H. J. Wang[34,j,k], H. P. Wang[1,58], K. Wang[1,53], L. L. Wang[1], M. Wang[45], M. Z. Wang[42,g], Meng Wang[1,58], S. Wang[10,f], S. Wang[13], T. Wang[10,f], T. J. Wang[39], W. Wang[54], W. H. Wang[71], W. P. Wang[66,53], X. Wang[42,g], X. F. Wang[34,j,k], X. L. Wang[10,f], Y. Wang[56], Y. D. Wang[41], Y. F. Wang[1,53,58], Y. H. Wang[43], Y. Q. Wang[1], Yaqian Wang[16,1], Z. Wang[1,53], Z. Y. Wang[1,58], Ziyi Wang[58], D. H. Wei[13], F. Weidner[63], S. P. Wen[1], D. J. White[62], U. Wiedner[4], G. Wilkinson[64], M. Wolke[70], L. Wollenberg[4], J. F. Wu[1,58], L. H. Wu[1], L. J. Wu[1,58], X. Wu[10,f], X. H. Wu[30], Y. Wu[66], Y. J Wu[28], Z. Wu[1,53], L. Xia[66,53], T. Xiang[42,g], D. Xiao[34,j,k], G. Y. Xiao[38], H. Xiao[10,f], S. Y. Xiao[1], Y. L. Xiao[10,f], Z. J. Xiao[37], C. Xie[38], X. H. Xie[42,g], Y. Xie[45], Y. G. Xie[1,53], Y. H. Xie[6], Z. P. Xie[66,53], T. Y. Xing[1,58], C. F. Xu[1], C. J. Xu[54], G. F. Xu[1], H. Y. Xu[61], Q. J. Xu[15], X. P. Xu[50], Y. C. Xu[58], Z. P. Xu[38], F. Yan[10,f], L. Yan[10,f], W. B. Yan[66,53], W. C. Yan[75], H. J. Yang[46,e], H. L. Yang[30], H. X. Yang[1], L. Yang[47], S. L. Yang[58], Tao Yang[1], Y. F. Yang[39], Y. X. Yang[1,58], Yifan Yang[1,58], M. Ye[1,53], M. H. Ye[8], J. H. Yin[1], Z. Y. You[54], B. X. Yu[1,53,58], C. X. Yu[39], G. Yu[1,58], T. Yu[67], C. Z. Yuan[1,58], L. Yuan[2], S. C. Yuan[1], X. Q. Yuan[1], Y. Yuan[1,58], Z. Y. Yuan[54], C. X. Yue[35], A. A. Zafar[68], F. R. Zeng[45], X. Zeng Zeng[6], Y. Zeng[23,h], Y. H. Zhan[54], A. Q. Zhang[1], B. L. Zhang[1], B. X. Zhang[1], D. H. Zhang[39], G. Y. Zhang[18], H. Zhang[66], H. H. Zhang[54], H. H. Zhang[30], H. Y. Zhang[1,53], J. L. Zhang[72], J. Q. Zhang[37], J. W. Zhang[1,53,58], J. X. Zhang[34,j,k], J. Y. Zhang[1], J. Z. Zhang[1,58], Jianyu Zhang[1,58], Jiawei Zhang[1,58], L. M. Zhang[56], L. Q. Zhang[54], Lei Zhang[38], P. Zhang[1], Q. Y. Zhang[35,75], Shuihan Zhang[1,58], Shulei Zhang[23,h], X. D. Zhang[41],

X. M. Zhang[1], X. Y. Zhang[50], X. Y. Zhang[45], Y. Zhang[64], Y. T. Zhang[75], Y. H. Zhang[1,53], Yan Zhang[66,53], Yao Zhang[1], Z. H. Zhang[1], Z. Y. Zhang[39], Z. Y. Zhang[71], G. Zhao[1], J. Zhao[35], J. Y. Zhao[1,58], J. Z. Zhao[1,53], Lei Zhao[66,53], Ling Zhao[1], M. G. Zhao[39], Q. Zhao[1], S. J. Zhao[75], Y. B. Zhao[1,53], Y. X. Zhao[28,58], Z. G. Zhao[66,53], A. Zhemchugov[32,a], B. Zheng[67], J. P. Zheng[1,53], Y. H. Zheng[58], B. Zhong[37], C. Zhong[67], X. Zhong[54], H. Zhou[45], L. P. Zhou[1,58], X. Zhou[71], X. K. Zhou[58], X. R. Zhou[66,53], X. Y. Zhou[35], Y. Z. Zhou[10,f], J. Zhu[39], K. Zhu[1], K. J. Zhu[1,53,58], L. X. Zhu[58], S. H. Zhu[65], S. Q. Zhu[38], T. J. Zhu[72], W. J. Zhu[10,f], Y. C. Zhu[66,53], Z. A. Zhu[1,58], B. S. Zou[1], J. H. Zou[1]

(BESIII Collaboration)

[1] *Institute of High Energy Physics, Beijing 100049, People's Republic of China*
[2] *Beihang University, Beijing 100191, People's Republic of China*
[3] *Beijing Institute of Petrochemical Technology, Beijing 102617, People's Republic of China*
[4] *Bochum Ruhr-University, D-44780 Bochum, Germany*
[5] *Carnegie Mellon University, Pittsburgh, Pennsylvania 15213, USA*
[6] *Central China Normal University, Wuhan 430079, People's Republic of China*
[7] *Central South University, Changsha 410083, People's Republic of China*
[8] *China Center of Advanced Science and Technology, Beijing 100190, People's Republic of China*
[9] *COMSATS University Islamabad, Lahore Campus, Defence Road, Off Raiwind Road, 54000 Lahore, Pakistan*
[10] *Fudan University, Shanghai 200433, People's Republic of China*
[11] *G.I. Budker Institute of Nuclear Physics SB RAS (BINP), Novosibirsk 630090, Russia*
[12] *GSI Helmholtzcentre for Heavy Ion Research GmbH, D-64291 Darmstadt, Germany*
[13] *Guangxi Normal University, Guilin 541004, People's Republic of China*
[14] *Guangxi University, Nanning 530004, People's Republic of China*
[15] *Hangzhou Normal University, Hangzhou 310036, People's Republic of China*
[16] *Hebei University, Baoding 071002, People's Republic of China*
[17] *Helmholtz Institute Mainz, Staudinger Weg 18, D-55099 Mainz, Germany*
[18] *Henan Normal University, Xinxiang 453007, People's Republic of China*
[19] *Henan University of Science and Technology, Luoyang 471003, People's Republic of China*
[20] *Henan University of Technology, Zhengzhou 450001, People's Republic of China*
[21] *Huangshan College, Huangshan 245000, People's Republic of China*
[22] *Hunan Normal University, Changsha 410081, People's Republic of China*
[23] *Hunan University, Changsha 410082, People's Republic of China*
[24] *Indian Institute of Technology Madras, Chennai 600036, India*
[25] *Indiana University, Bloomington, Indiana 47405, USA*
[26] *INFN Laboratori Nazionali di Frascati , (A)INFN Laboratori Nazionali di Frascati, I-00044, Frascati, Italy; (B)INFN Sezione di Perugia, I-06100, Perugia, Italy; (C)University of Perugia, I-06100, Perugia, Italy*
[27] *INFN Sezione di Ferrara, (A)INFN Sezione di Ferrara, I-44122, Ferrara, Italy; (B)University of Ferrara, I-44122, Ferrara, Italy*
[28] *Institute of Modern Physics, Lanzhou 730000, People's Republic of China*
[29] *Institute of Physics and Technology, Peace Avenue 54B, Ulaanbaatar 13330, Mongolia*
[30] *Jilin University, Changchun 130012, People's Republic of China*
[31] *Johannes Gutenberg University of Mainz, Johann-Joachim-Becher-Weg 45, D-55099 Mainz, Germany*
[32] *Joint Institute for Nuclear Research, 141980 Dubna, Moscow region, Russia*
[33] *Justus-Liebig-Universitaet Giessen, II. Physikalisches Institut, Heinrich-Buff-Ring 16, D-35392 Giessen, Germany*
[34] *Lanzhou University, Lanzhou 730000, People's Republic of China*
[35] *Liaoning Normal University, Dalian 116029, People's Republic of China*
[36] *Liaoning University, Shenyang 110036, People's Republic of China*
[37] *Nanjing Normal University, Nanjing 210023, People's Republic of China*
[38] *Nanjing University, Nanjing 210093, People's Republic of China*
[39] *Nankai University, Tianjin 300071, People's Republic of China*
[40] *National Centre for Nuclear Research, Warsaw 02-093, Poland*
[41] *North China Electric Power University, Beijing 102206, People's Republic of China*
[42] *Peking University, Beijing 100871, People's Republic of China*
[43] *Qufu Normal University, Qufu 273165, People's Republic of China*
[44] *Shandong Normal University, Jinan 250014, People's Republic of China*
[45] *Shandong University, Jinan 250100, People's Republic of China*
[46] *Shanghai Jiao Tong University, Shanghai 200240, People's Republic of China*
[47] *Shanxi Normal University, Linfen 041004, People's Republic of China*
[48] *Shanxi University, Taiyuan 030006, People's Republic of China*
[49] *Sichuan University, Chengdu 610064, People's Republic of China*
[50] *Soochow University, Suzhou 215006, People's Republic of China*
[51] *South China Normal University, Guangzhou 510006, People's Republic of China*
[52] *Southeast University, Nanjing 211100, People's Republic of China*
[53] *State Key Laboratory of Particle Detection and Electronics, Beijing 100049, Hefei 230026, People's Republic of China*

[54] Sun Yat-Sen University, Guangzhou 510275, People's Republic of China

[55] Suranaree University of Technology, University Avenue 111, Nakhon Ratchasima 30000, Thailand

[56] Tsinghua University, Beijing 100084, People's Republic of China

[57] Turkish Accelerator Center Particle Factory Group, (A)Istinye University, 34010, Istanbul, Turkey; (B)Near East University, Nicosia, North Cyprus, Mersin 10, Turkey

[58] University of Chinese Academy of Sciences, Beijing 100049, People's Republic of China

[59] University of Groningen, NL-9747 AA Groningen, The Netherlands

[60] University of Hawaii, Honolulu, Hawaii 96822, USA

[61] University of Jinan, Jinan 250022, People's Republic of China

[62] University of Manchester, Oxford Road, Manchester, M13 9PL, United Kingdom

[63] University of Muenster, Wilhelm-Klemm-Strasse 9, 48149 Muenster, Germany

[64] University of Oxford, Keble Road, Oxford OX13RH, United Kingdom

[65] University of Science and Technology Liaoning, Anshan 114051, People's Republic of China

[66] University of Science and Technology of China, Hefei 230026, People's Republic of China

[67] University of South China, Hengyang 421001, People's Republic of China

[68] University of the Punjab, Lahore-54590, Pakistan

[69] University of Turin and INFN, (A)University of Turin, I-10125, Turin, Italy; (B)University of Eastern Piedmont, I-15121, Alessandria, Italy; (C)INFN, I-10125, Turin, Italy

[70] Uppsala University, Box 516, SE-75120 Uppsala, Sweden

[71] Wuhan University, Wuhan 430072, People's Republic of China

[72] Xinyang Normal University, Xinyang 464000, People's Republic of China

[73] Yunnan University, Kunming 650500, People's Republic of China

[74] Zhejiang University, Hangzhou 310027, People's Republic of China

[75] Zhengzhou University, Zhengzhou 450001, People's Republic of China

[a] Also at the Moscow Institute of Physics and Technology, Moscow 141700, Russia

[b] Also at the Novosibirsk State University, Novosibirsk, 630090, Russia

[c] Also at the NRC "Kurchatov Institute", PNPI, 188300, Gatchina, Russia

[d] Also at Goethe University Frankfurt, 60323 Frankfurt am Main, Germany

[e] Also at Key Laboratory for Particle Physics, Astrophysics and Cosmology, Ministry of Education; Shanghai Key Laboratory for Particle Physics and Cosmology; Institute of Nuclear and Particle Physics, Shanghai 200240, People's Republic of China

[f] Also at Key Laboratory of Nuclear Physics and Ion-beam Application (MOE) and Institute of Modern Physics, Fudan University, Shanghai 200443, People's Republic of China

[g] Also at State Key Laboratory of Nuclear Physics and Technology, Peking University, Beijing 100871, People's Republic of China

[h] Also at School of Physics and Electronics, Hunan University, Changsha 410082, China

[i] Also at Guangdong Provincial Key Laboratory of Nuclear Science, Institute of Quantum Matter, South China Normal University, Guangzhou 510006, China

[j] Also at Frontiers Science Center for Rare Isotopes, Lanzhou University, Lanzhou 730000, People's Republic of China

[k] Also at Lanzhou Center for Theoretical Physics, Lanzhou University, Lanzhou 730000, People's Republic of China

[l] Also at the Department of Mathematical Sciences, IBA, Karachi , Pakistan

The radiative hyperon decay $\Lambda \to n\gamma$ is studied using $(10087 \pm 44) \times 10^6$ J/ψ events collected with the BESIII detector operating at BEPCII. The absolute branching fraction of the decay $\Lambda \to n\gamma$ is determined with a significance of 5.6σ to be $[0.832 \pm 0.038(\text{stat.}) \pm 0.054(\text{syst.})] \times 10^{-3}$, which lies significantly below the current PDG value. By analyzing the joint angular distribution of the decay products, the first determination of the decay asymmetry α_γ is reported with a value of $-0.16 \pm 0.10(\text{stat.}) \pm 0.05(\text{syst.})$.

Weak radiative transitions of hadrons are governed by the interplay of the electromagnetic, weak, and strong interactions [1] and involve parity violating (p.v.) and parity conserving (p.c.) amplitudes. According to Hara's theorem [2], the p.v. amplitude of radiative hyperon decays, $B_i \to B_f\gamma$, vanishes in the limit of SU(3) flavor symmetry. Taking into account the breaking of this symmetry in the quark model, the decay asymmetry α_γ, given by the interference between p.v. and p.c. amplitudes, is expected to be positive for decays such as $\Sigma^+ \to p\gamma$, where the s quark in the initial state baryon decays to a d quark. It was, therefore, a surprise when several experiments reported a large negative value of the decay

asymmetry for this process [3–7]. For other radiative hyperon decays, measurements have found non-vanishing positive decay asymmetries [8, 9]. The disagreement between theoretical expectation and experimental results provoked wide interest in these processes, and various solutions to the puzzle were proposed [10–16]. It was suggested that the validity of Hara's theorem could be confirmed by determining the sign of the $\Lambda \to n\gamma$ decay asymmetry [17], a positive value indicating the theorem's violation [18–20].

In the three previous measurements of $\Lambda \to n\gamma$ performed by two fixed target experiments [21–23], the branching fraction (BF) was obtained from the ratio

$\mathcal{B}_{\Lambda\to n\gamma}/\mathcal{B}_{\Lambda\to n\pi^0}$. Only the result from Ref. [23] is considered by the Particle Data Group (PDG) [24]. The decay asymmetry of $\Lambda \to n\gamma$, however, which is essential for the test of the Hara theorem, has not been measured so far.

At BESIII, a measurement of the $\Lambda \to n\gamma$ decay utilizing the large yield of $\Lambda\bar{\Lambda}$ pairs from $J/\psi \to \Lambda\bar{\Lambda}$ [25] is accomplished using a double-tag (DT) technique [26]. The $J/\psi \to \Lambda\bar{\Lambda}$ events are identified by reconstructing the pionic decay $\bar{\Lambda} \to \bar{p}\pi^+$ ($\Lambda \to p\pi^-$), denoted as single-tag (ST). Then a DT event consisting of an ST $\bar{\Lambda}$ (Λ) candidate accompanied with a $\Lambda \to n\gamma$ ($\bar{\Lambda} \to \bar{n}\gamma$) candidate is selected. The absolute BF of the decay $\Lambda \to n\gamma$ is given by

$$\mathcal{B}_{\Lambda\to n\gamma} = \frac{N_{\mathrm{DT}}/\varepsilon_{\mathrm{DT}}}{N_{\mathrm{ST}}/\varepsilon_{\mathrm{ST}}}, \qquad (1)$$

where N_{ST} (N_{DT}) and $\varepsilon_{\mathrm{ST}}$ ($\varepsilon_{\mathrm{DT}}$) are the ST (DT) yield and the corresponding detection efficiency. Here and throughout this letter, charge-conjugate channels are implied unless stated otherwise.

A previous BESIII study [27] showed that the Λ from $J/\psi \to \Lambda\bar{\Lambda}$ is transversely polarized with a magnitude reaching 25%. This polarization can be used to determine the decay asymmetry α_γ in the $\Lambda \to n\gamma$ decay from the angular distribution of the daughter baryons from the $J/\psi \to \Lambda\bar{\Lambda}$ process [28]. Generally, the joint angular distribution $\mathcal{W}$ of $J/\psi \to \bar{\Lambda}(\to \bar{p}\pi^+)\Lambda(\to n\gamma)$ can be expressed as:

$$\begin{aligned}
&\mathcal{W}\left(\xi; \alpha_\psi, \Delta\Phi, \alpha_\gamma, \alpha_+\right)\\
&= 1 + \alpha_\psi \cos^2\theta_\Lambda + \alpha_\gamma\alpha_+ \left[\sin^2\theta_\Lambda \left(n_1^x n_2^x - \alpha_\psi n_1^y n_2^y\right)\right.\\
&\left.+ \left(\cos^2\theta_\Lambda + \alpha_\psi\right) n_1^z n_2^z\right]\\
&+ \alpha_\gamma\alpha_+\sqrt{1-\alpha_\psi^2}\cos(\Delta\Phi)\sin\theta_\Lambda\cos\theta_\Lambda\left(n_1^x n_2^z + n_1^z n_2^x\right)\\
&+ \sqrt{1-\alpha_\psi^2}\sin(\Delta\Phi)\sin\theta_\Lambda\cos\theta_\Lambda\left(\alpha_\gamma n_1^y + \alpha_+ n_2^y\right),
\end{aligned} \qquad (2)$$

where $\hat{\mathbf{n}}_1$ ($\hat{\mathbf{n}}_2$) is the unit vector in the direction of the neutron (anti-proton) in the Λ ($\bar{\Lambda}$) rest frame. The components of $\hat{\mathbf{n}}_1$ and $\hat{\mathbf{n}}_2$ are (n_1^x, n_1^y, n_1^z) and (n_2^x, n_2^y, n_2^z), in a coordinate system where the z axis of both the Λ and the $\bar{\Lambda}$ rest frame is oriented along the momentum $\mathbf{p}_\Lambda$ at an angle θ_Λ with respect to the e^- beam direction. The y axis is perpendicular to the production plane and oriented along the vector $\mathbf{k}_- \times \mathbf{p}_\Lambda$, where $\mathbf{k}_-$ is the e^- beam momentum in the J/ψ rest frame. For each event, the full set of kinematic variables $(\theta_\Lambda, \hat{\mathbf{n}}_1, \hat{\mathbf{n}}_2)$ is denoted by ξ. Furthermore, α_ψ and $\Delta\Phi$ denote the absolute ratio of the two helicity amplitudes of $J/\psi \to \Lambda\bar{\Lambda}$ and their relative phase, respectively, and α_γ (α_+) is the decay asymmetry of $\Lambda \to n\gamma$ ($\bar{\Lambda} \to \bar{p}\pi^+$).

In this letter, we report the absolute BF and the decay asymmetry of $\Lambda \to n\gamma$ from $(10087 \pm 44) \times 10^6$ J/ψ events [29] collected at the BESIII detector [30, 31] operating at the BEPCII collider [32]. A detailed description of the BESIII detector can be found

in Ref. [30]. Simulated data samples produced with GEANT4-based [33] Monte Carlo (MC) software, including a detailed geometric description of the BESIII detector and the detector response, are used to determine detection efficiencies and estimate background contributions. The J/ψ resonance is generated by KKMC [34], incorporating the effects of the beam energy spread and the initial state radiation in the e^+e^- annihilation. The subsequent decays are modeled with EvtGen [35] using the BFs taken from the PDG [24] for known decays and LundCharm [36] for remaining unknown decays. A sample of simulated J/ψ decay events (the inclusive MC sample), corresponding to the luminosity of data, is used to study background events. Signal MC samples, including a sample of 5.6×10^7 $J/\psi \to \bar{\Lambda}(\to \bar{p}\pi^+)\Lambda(\to \text{anything})$ and a sample of 4×10^5 $J/\psi \to \bar{\Lambda}(\to \bar{p}\pi^+)\Lambda(\to n\gamma)$, are generated to estimate the ST and DT signal efficiencies, respectively. The joint angular distributions are generated according to Eq. (2), where α_γ is adopted from this analysis and $\alpha_\psi = 0.461 \pm 0.006 \pm 0.007$, $\Delta\Phi = 42.4 \pm 0.6 \pm 0.5°$ and $\alpha_+ = -0.758 \pm 0.010 \pm 0.007$ from Ref. [27]. Moreover, a sample of 2×10^7 $J/\psi \to \bar{\Lambda}(\to \bar{p}\pi^+)\Lambda(\to n\pi^0)$ events is generated to study the dominant background.

The ST $\bar{\Lambda}$ candidate is reconstructed through the dominant decay mode $\bar{\Lambda} \to \bar{p}\pi^+$. Charged tracks are detected in the main drift chamber (MDC) and must satisfy the condition $|\cos\theta| < 0.93$, where θ is the polar angle with respect to the MDC symmetry axis. The momenta ranges of pions and anti-protons from the $\bar{\Lambda}$ decays are well separated, thus the tracks with momenta less than 0.5 GeV/c are assigned to be pions, otherwise anti-protons. In addition, measurements of the specific ionization energy loss in the MDC and the flight time by the time-of-flight system are combined to perform particle identification for the (anti-)proton candidate. They are required to have the largest likelihood for the particle type selected among the pion, kaon and proton hypotheses. Events with at least one anti-proton and one positively charged pion are selected. A vertex fit is performed to each $\bar{p}\pi^+$ pair, and the one with the minimum χ^2_{vtx} of the vertex fit is regarded as the $\bar{\Lambda}$ candidate for further analysis. The $\bar{\Lambda}$ candidate is required to have χ^2_{vtx} less than 20, an invariant mass within 8 MeV/c^2 of the nominal Λ mass [24] and a decay length relative to the interaction point larger than twice of its resolution.

To identify events with $J/\psi \to \Lambda\bar{\Lambda}$ and reduce the background contributions from $J/\psi \to \bar{\Lambda} + $ anything which are not due to $J/\psi \to \Lambda\bar{\Lambda}$, a recoil mass $M_{\bar{\Lambda}}^{\mathrm{rec}} = \sqrt{(E_{\mathrm{c.m.}} - E_{\bar{\Lambda}})^2 - P_{\bar{\Lambda}}^2}$ is defined, where $E_{\mathrm{c.m.}}$ is the center-of-mass (c.m.) energy, $E_{\bar{\Lambda}}$ is the energy and $P_{\bar{\Lambda}}$ the momentum of the ST $\bar{\Lambda}$ candidate. This mass is required to be within $1.03 < M_{\bar{\Lambda}}^{\mathrm{rec}} < 1.18$ GeV/c^2. The distribution of $M_{\bar{\Lambda}}^{\mathrm{rec}}$ is shown in Fig. 1, where only few background events are observed. A maximum likelihood fit is performed to determine the signal yield, where the signal and background distributions are represented by

shapes obtained from signal MC and inclusive MC samples. The MC shapes are convolved with a Gaussian function to account for imperfect simulation of the detector resolution. The charge conjugate channels are analyzed with the duplicate processing method, and the yields of ST Λ and $\bar{\Lambda}$ candidates from the fits are summarized in Table I. The background contribution is less than 1%, which is also validated by the inclusive MC sample.
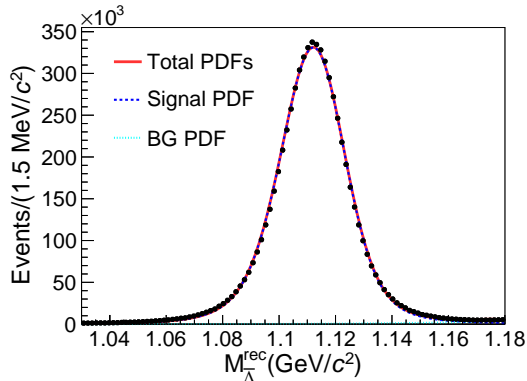
FIG. 1. Distribution of the recoil mass $M_{\bar{\Lambda}}^{\rm rec}$ after ST selection. The black dots with error bars represent data, the error bars are smaller than the marker size. The red solid line shows the fit result and the blue dashed and cyan dotted lines are the signal and background distributions, respectively.

On the signal side we search for $\Lambda \to n\gamma$ from the residual neutral particles in the ST $\bar{\Lambda}$ candidates. For a neutral shower, the deposited energy in the electromagnetic calorimeter (EMC) should be larger than 25 MeV in the barrel region ($|\cos\theta| < 0.80$) or 50 MeV in the end cap region ($0.86 < |\cos\theta| < 0.92$). To reject secondary showers originating from charged tracks, the shower candidates are required to be apart from the charged tracks with an opening angle of $10°$ for pion and proton tracks and $20°$ for anti-proton tracks. To suppress electronic noise, the interval between the EMC response time and the event start time is required to be within 700 ns. There are two neutral particles in the final states of the signal process $\Lambda \to n\gamma$ ($\bar{\Lambda} \to \bar{n}\gamma$), the photon and the (anti-)neutron. The radiative photon produces a shower in the EMC with deposited energy less than 400 MeV. With a probability of 0.65, the $\bar{n}$ annihilates in the EMC and produces several secondary particles. The most energetic shower with energy deposit larger than 0.4 GeV is regarded as an $\bar{n}$ candidate. The n, meanwhile, is difficult to identify due to its low interaction efficiency and its small energy deposition, and is treated as a missing particle. Therefore, only the γs and $\bar{n}$ are selected in this analysis. At least one shower is required as a γ candidate in an event for $\Lambda \to n\gamma$, and at least two showers as γ and $\bar{n}$ in an event for $\bar{\Lambda} \to \bar{n}\gamma$. For the reconstruction of $\Lambda \to n\gamma$, a one-constraint (1C) kinematic fit is applied by imposing energy-momentum conservation of the candidate particles in the hypothetical $J/\psi \to \bar{\Lambda}n\gamma$ process, where the neutron is set as a missing particle.

On the other hand, for the reconstruction of $\bar{\Lambda} \to \bar{n}\gamma$, a 3C kinematic fit is imposed for the $J/\psi \to \Lambda\bar{n}\gamma$ process, where the direction of the $\bar{n}$ is measured and the energy is unmeasured. For events with multiple photon candidates, the combination giving the minimum χ_{1C}^2 (χ_{3C}^2) is retained for the analysis. Furthermore, χ_{1C}^2 (χ_{3C}^2) is required to be less than 10 (15).

Detailed MC studies show that the dominant background contribution comes from the $\Lambda \to n\pi^0$ decay with its large BF, while other background processes are almost negligible. The background can be classified into two categories: first, events with the detected photon from the π^0 decay in $\Lambda \to n\pi^0$, denoted as BG A, and second, events with the detected photon not from the π^0 decay, denoted as BG B. In the latter case, the photons arise from noise or a shower from secondary products of other particles. In order to suppress BG A, a 1C (3C) kinematic fit under the hypothesis $J/\psi \to \bar{\Lambda}n\gamma\gamma$ ($J/\psi \to \Lambda\bar{n}\gamma\gamma$) is performed, and events surviving the kinematic fit and with a $\gamma\gamma$ invariant mass within 20 MeV/c^2 of the π^0 nominal mass [24] are rejected. To suppress BG B, the detected photon is required to have an energy larger than 150 MeV and an opening angle larger than $20°$ from the (anti-)neutron candidate. Additionally, for BG A and BG B a boosted decision tree (BDT) is applied on the detected photon to discriminate signal photons from other showers, based on the measured variables, $i.e.$ deposited energy, secondary moment, number of hits, Zernike moment (A_{42}), and deposition shape [37]. The response of the BDT output is required to be larger than 0.3, after which 86.8% (92.8%) of the BG A and 99.5% (99.7%) of the BG B events are rejected with 44.6% (48.4%) loss of the signal efficiency for the $\Lambda \to n\gamma$ ($\bar{\Lambda} \to \bar{n}\gamma$) process.

The distribution of the photon energy in the Λ rest frame E_γ^Λ after all selection criteria is shown in Fig. 2 for the decay $\Lambda \to n\gamma$ ($\bar{\Lambda} \to \bar{n}\gamma$), where the predominant peak around 0.13 GeV is from BG A, and the second peak around 0.15 GeV corresponds to the signal. To determine the DT signal yields, an unbinned extended maximum likelihood fit is performed to the E_γ^Λ distributions. The signal and BG A are modeled by the MC simulated shape convolved with a Gaussian function. Since BG B involves a fake photon and is difficult to be modeled by the MC simulation, its lineshape is obtained by a data-driven approach with a control sample of $\Lambda \to n\pi^0(\to \gamma\gamma)$, and the photon candidates used in the kinematic fit are from noise photons in the EMC rather than the two signal photons from $\pi^0 \to \gamma\gamma$. The DT yields obtained from fits are summarized in Table I. The BFs determined according to Eq. (1) are found to be consistent for the two charge-conjugate modes. Therefore, a simultaneous fit, assuming the same BF for the two modes, is performed, and the results are given in bold font in the Table I.

The systematic uncertainties on the BF measurement stem from the photon and anti-neutron detection efficiency, kinematic fit, invariant $M_{\gamma\gamma}$ mass selection window, opening angle between photon and (anti-)neutron,
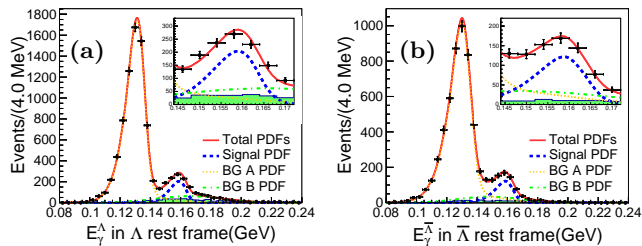
FIG. 2. Distributions of E_γ^Λ for (a) $\Lambda \to n\gamma$ and (b) $\bar{\Lambda} \to \bar{n}\gamma$ in the Λ and $\bar{\Lambda}$ rest frame, respectively. The black dots with error bars represent data. The red solid, blue dashed, orange dotted, and green dash-dotted lines denote the fit result, signal, BG A, and BG B contributions, respectively. The green histograms indicate the BG B from an inclusive MC sample. The insets show the details of the fit in the signal region.

TABLE I. The results for the decays $\Lambda \to n\gamma$ and $\bar{\Lambda} \to \bar{n}\gamma$. The BF and α_γ values are given both for individual and simultaneous fits. The first (second) uncertainties are statistical (systematic).

Decay Mode	$\Lambda \to n\gamma$	$\bar{\Lambda} \to \bar{n}\gamma$
N_{ST} $(\times 10^3)$	6853.2 ± 2.6	7036.2 ± 2.7
$\varepsilon_{\mathrm{ST}}$ (%)	51.13 ± 0.01	52.53 ± 0.01
N_{DT}	723 ± 40	498 ± 41
$\varepsilon_{\mathrm{DT}}$ (%)	6.58 ± 0.04	4.32 ± 0.03
BF $(\times 10^{-3})$	$0.820 \pm 0.045 \pm 0.066$	$0.862 \pm 0.071 \pm 0.084$
	$0.832 \pm 0.038 \pm 0.054$	
α_γ	$-0.13 \pm 0.13 \pm 0.03$	$0.21 \pm 0.15 \pm 0.06$
	$-0.16 \pm 0.10 \pm 0.05$	

BDT output for the photon, MC model due to α_γ, and fit procedure. The uncertainties associated with ST selection almost cancel based on Eq. (1). There is only one photon for the signal process, and the uncertainty associated with the photon detection efficiency is 1% according to Ref. [38]. The uncertainty of the anti-neutron detection efficiency is negligible after correcting the efficiency by a data-driven method [39]. To estimate the uncertainty due to the kinematic fit, we change the value of the $\chi^2_{1\mathrm{C}}$ ($\chi^2_{3\mathrm{C}}$) by ± 1 and investigate the fluctuation on the BF, which is taken as a systematic uncertainty. The uncertainty from the $M(\gamma\gamma)$ mass window requirement is studied with the control sample of $J/\psi \to \bar{\Lambda}\ (\to \bar{p}\pi^+)\Lambda\ (\to n\pi^0)\pi^0\ (\to \gamma\gamma)$, and the difference of the efficiency between the data and MC simulation, 1.2%, is taken as the uncertainty. The uncertainty from the requirement of the opening angle between photon and (anti-)neutron is estimated to be 2.0% by varying the selection criteria by two degrees. The uncertainty associated with the BDT for the photon is negligible after correcting the efficiency using the control sample of $J/\psi \to \rho\pi\ (\to \pi^+\pi^-\gamma\gamma)$. The uncertainty of the MC model due to the input decay asymmetry α_γ is estimat-

ed to be 0.6% by varying the input value of α_γ by its uncertainty. The systematic uncertainties from the fit of the E_γ^Λ distribution include those associated with the fit range and the modeling of the signal and background shapes. An alternative fit of the E_γ^Λ distribution in the $(0.09, 0.23)$ GeV range is performed, and the resultant difference in signal yield, 0.3%, is taken as the uncertainty. The uncertainties associated with the shape modeling of the signal and BG A, are estimated by varying the width of the Gaussian resolution function within the uncertainties. The resulting differences of the yields, 0.4% for the signal and 1.0% for BG A, are assigned as the systematic uncertainties. To estimate the shape modeling uncertainty of BG B, ensembles of pseudo-data are generated according to modified BG B distributions as allowed by the uncertainties, and the resulting standard deviation of the signal yields, 4.8%, is taken as the systematic uncertainty. The systematic uncertainty associated with the extraction of the ST yield is estimated by varying the width of the Gaussian resolution function within its uncertainties for signal shape modeling and replacing the inclusive MC shape with a second order polynomial function. The resulting difference in the ST yield of 2.3% is taken as the systematic uncertainty. By adding all these values in quadrature, the total systematic uncertainty is estimated to be 6.5%.

The decay asymmetry α_γ is determined using Eq. (2) with a maximum likelihood fit. A total of 1994 candidate events within a range of $(0.145, 0.17)$ GeV around E_γ^Λ are used in the fit, with an estimated fraction of background events of 43.3%. In the fit of α_γ, the likelihood function of the i-th event is calculated through the probability density function (PDF):

$$\mathcal{P}(\xi^i; \alpha_\psi, \Delta\Phi, \alpha_\gamma, \alpha_+) = \mathcal{CW}(\xi^i; \alpha_\psi, \Delta\Phi, \alpha_\gamma, \alpha_+)\epsilon(\xi^i), \tag{3}$$

where $\mathcal{C}^{-1} = \int \mathcal{W}(\xi; \alpha_\psi, \Delta\Phi, \alpha_\gamma, \alpha_+)\epsilon(\xi)d\xi$ is the normalization factor evaluated by a phase space (PHSP) MC sample, and $\alpha_\psi, \Delta\Phi, \alpha_+$ are fixed to the values in Ref. [27]. The BG A and BG B contributions to the likelihood value are estimated with MC samples and subtracted in the calculation of the likelihood function. We fit the $\Lambda \to n\gamma$ and $\bar{\Lambda} \to \bar{n}\gamma$ decay modes individually, and the results agree within statistical uncertainties as summarized in Table I. A simultaneous fit, assuming the same magnitude of α_γ but with opposite sign for the charge-conjugate modes, is used to determine the decay asymmetry, yielding $\alpha_\gamma(\Lambda \to n\gamma) = -0.16 \pm 0.10$, where the uncertainty is statistical. The polarization is strongly dependent on the Λ direction $\cos\theta_\Lambda$ and indicates the amplitude of the decay asymmetry. The n_1^y (n_2^y) moment

$$\mu(\cos\theta_\Lambda) = \frac{m}{N}\sum_{i=1}^{N_k} n_{1(2)}^y, \tag{4}$$

is proportional to the product of the Λ polarization and its decay asymmetry. It is calculated for $m = 10$ bins

in $\cos\theta_\Lambda$. Here, N is the total number of events in the data sample and N_k is the number of events in the k-th $\cos\theta_\Lambda$ bin. Figure 3 shows the projection of the global fit together with data and PHSP MC results. The fit result for $\bar\Lambda \to \bar p\pi^+$ clearly deviates from the PHSP curve while the one for $\Lambda \to n\gamma$ is consistent with PHSP. The difference in magnitude of the moments for $\bar\Lambda \to \bar p\pi^+$ and $\Lambda \to n\gamma$ implies different values of the decay asymmetries since the polarization is the same for $\bar\Lambda$ and Λ.
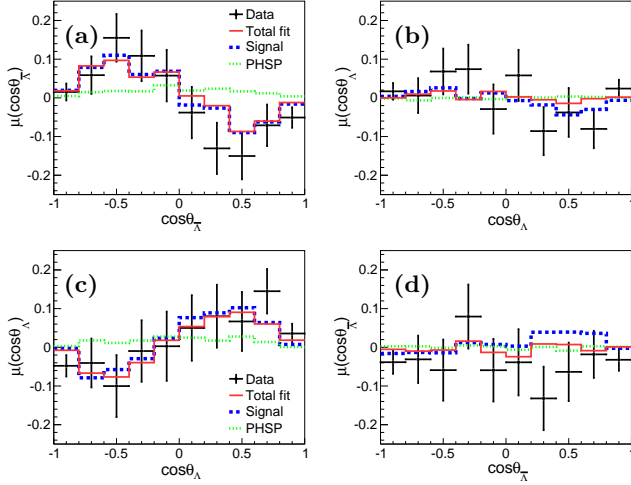
FIG. 3. Polarization moment $\mu(\cos\theta_{\bar\Lambda(\Lambda)})$ vs $\cos\theta_{\bar\Lambda(\Lambda)}$ for (a) $\bar\Lambda \to \bar p\pi^+$, (b) $\Lambda \to n\gamma$ in the process $J/\psi \to \bar\Lambda \, (\to \bar p\pi^+)\Lambda \, (\to n\gamma)$, and moment distribution $\mu(\cos\theta_{\Lambda(\bar\Lambda)})$ vs $\cos\theta_{\Lambda(\bar\Lambda)}$ for (c) $\Lambda \to p\pi^-$ and (d) $\bar\Lambda \to \bar n\gamma$ in the process $J/\psi \to \Lambda \, (\to p\pi^-)\bar\Lambda \, (\to \bar n\gamma)$. Dots with error bars indicate data and red solid lines show the fit result. The blue dashed and green dotted lines represent the moment for signal and PHSP MC, respectively.

The systematic uncertainties on α_γ are calculated as in the BF measurement except for the detection of photon and anti-neutron, as well as the BDT requirements, which are expected to be negligible. All the individual uncertainties are estimated by alternative unbinned maximum likelihood fits with the different scenarios, and the resultant (maximum) change on α_γ is assigned as the corresponding uncertainty. The uncertainty from the 1C (3C) kinematic fit is 0.024 (0.022), which is estimated by varying the selection criteria of χ^2_{1C} (χ^2_{3C}). The uncertainty associated with the requirement on the invariant $M_{\gamma\gamma}$ mass window is 0.016 estimated by varying the mass window from 20 to 27 MeV/c^2. The uncertainty due to the requirement of the opening angle between photon and (anti-)neutron is 0.028 estimated by varying the corresponding selection criteria. The uncertainty associated with the signal and background magnitudes, which are determined by the fit of the E_γ^Λ distribution, is estimated with the same approaches as in the BF measurement by changing the fit range, the signal modeling, BG A and BG B modeling, and the resultant differences with

respect to the nominal α_γ value. The obtained uncertainties are 0.001, 0.001, 0.002, and 0.008, respectively. The uncertainty due to the fixed parameters ($\alpha_\psi, \Delta\Phi, \alpha_-, \alpha_+$) in the fit is estimated by varying each parameter by its resolution, and the resulting differences 0.004, 0.09, 0.00, 0.03 are assigned as the uncertainties. The total systematic uncertainty of α_γ is estimated to be 0.05 by adding all these uncertainties in quadrature.

In summary, based on the double-tag method, we report the first measurement of the absolute BF of $\Lambda \to n\gamma$ of $[0.832 \pm 0.038(\text{stat.}) \pm 0.054(\text{syst.})] \times 10^{-3}$. The measured value of the BF is a factor of two smaller than the previous measurement of $(1.75 \pm 0.15) \times 10^{-3}$ [23]. By analyzing the joint angular distribution of the decay products, the decay asymmetry α_γ is determined for the first time, at a value of $-0.16 \pm 0.10(\text{stat.}) \pm 0.05(\text{syst.})$.

This analysis is the first measurement of radiative hyperon decays at an electron–positron collider experiment, making use of the huge number of polarized hyperons produced in J/ψ decays with clean background. The results for the asymmetry do not agree well with predictions such as the broken SU(3) pole model [19], Chiral Perturbation Theory [40], or the non-relativistic constituent quark model [20]. Our BF value is consistent with the lower unitary bound obtained by considering contributions of $\Lambda \to p\pi^-$ and $\Lambda \to n\pi^0$ weak hadronic decays together with $p\pi^- \to n\gamma$ and $n\pi^0 \to n\gamma$ rescattering, respectively [41].

---

[1] J. Lach and P. Zenczykowski, Int. J. Mod. Phys. A **10**, 3817 (1995).

[2] Y. Hara, Phys. Rev. Lett. **12**, 378 (1964).

[3] A. Manz, S. Reucroft, R. Settles, G. Wolf, J. Marraffino, C. Roos, J. Waters, and M. Webster, Phys. Lett. B **96**, 217 (1980).

[4] M. Kobayashi, J. Haba, T. Homma, H. Kawai, K. Miyake, T. S. Nakamura, N. Sasao, and Y. Sugimoto, Phys. Rev. Lett. **59**, 868 (1987).

[5] M. Foucher et al. (E761 Collaboration), Phys. Rev. Lett. **68**, 3004 (1980).

[6] M. Foucher et al., Phys. Rev. Lett. **68**, 3004 (1992).

[7] S. Timm et al. (E761 Collaboration), Phys. Rev. D **51**, 4638 (1995).

[8] C. James et al., Phys. Rev. Lett. **64**, 843 (1990).

[9] S. Teige et al., Phys. Rev. Lett. **63**, 2717 (1989).

[10] N. Vasanti, Phys. Rev. D **13**, 1889 (1976).

[11] Y. I. Kogan and M. A. Shifman, Sov. J. Nucl. Phys. **38**, 628 (1983).

[12] F. J. Gilman and M. B. Wise, Phys. Rev. D **19**, 976 (1979).

[13] C. Goldman and C. O. Escobar, Phys. Rev. D **40**, 106 (1989).

[14] M. D. Scadron and M. Visinescu, Phys. Rev. D **28**, 1117 (1983).

[15] D. Palle, Phys. Rev. D **36**, 2863 (1987).

[16] P. Zenczykowski, Phys. Rev. D **44**, 1485 (1991).

[17] P. Zenczykowski, Acta Phys. Polon. B **51**, 2111 (2020).

[18] M. B. Gavela, A. Le Yaouanc, L. Oliver, O. Pene, J. C. Raynal, and T. N. Pham, Phys. Lett. B **101**, 417 (1981).

[19] P. Zenczykowski, Phys. Rev. D **73**, 076005 (2006).

[20] P. Y. Niu, J. M. Richard, Q. Wang, and Q. Zhao, Chin. Phys. C **45**, 013101 (2021).

[21] S. F. Biagi et al., Z. Phys. C **30**, 201 (1986).

[22] A. J. Noble et al., Phys. Rev. Lett. **69**, 414 (1992).

[23] K. D. Larson et al., Phys. Rev. D **47**, 799 (1993).

[24] P. A. Zyla et al. (Particle Data Group), PTEP **2020**, 083C01 (2020).

[25] H. B. Li, Front. Phys. **12**, 121301 (2017), [Erratum: Front.Phys.(Beijing) 14, 64001 (2019)].

[26] R. M. Baltrusaitis et al. (MARK-III Collaboration), Phys. Rev. Lett. **56**, 2140 (1986).

[27] M. Ablikim et al. (BESIII Collaboration), Nature Physics **15**, 631 (2019).

[28] G. Fäldt and A. Kupsc, Phys. Lett. B **772**, 16 (2017).

[29] M. Ablikim et al. (BESIII Collaboration), arXiv e-prints , arXiv:2111.07571 (2021).

[30] M. Ablikim et al., Nucl. Instrum. Meth. A **614**, 345 (2010).

[31] M. Ablikim et al. (BESIII Collaboration), Chin. Phys. C **44**, 040001 (2020).

[32] C. Yu et al., in 7th International Particle Accelerator Conference (2016) p. TUYA01.

[33] S. Agostinelli et al., Nucl. Instrum. Meth. A **506**, 250 (2003).

[34] S. Jadach, B. F. L. Ward, and Z. Was, Phys. Rev. D **63**, 113009 (2001).

[35] D. J. Lange, Nucl. Instrum. Meth. A **462**, 152 (2001); R. G. Ping, Chin. Phys. C **32**, 599 (2008).

[36] J. C. Chen, G. S. Huang, X. R. Qi, D. H. Zhang, and Y. S. Zhu, Phys. Rev. D **62**, 034003 (2000); R. L. Yang, R. G. Ping, and H. Chen, Chin. Phys. Lett. **31**, 061301 (2014).

[37] The deposited energy is the total cluster energy of a shower, denoted as E_{tot}. The hit number is the total number of the ignited crystals of a shower. The secondary moment is defined as $\sum_i \frac{E_i r_i^2}{E_{tot}}$ and the Zernike moment(A_{42}) is defined as $|\sum_i \frac{E_i}{E_{tot}} f_{4,2}(\frac{r_i}{R_0}) e^{im\phi_i}|$ with the coefficient $f_{4,2} = 4x^4 - 3x^2$, where r_i and ϕ_i are the radial and angular seperation of crystal i with respect to the cluster center, E_i is the i_{th} ignited crystals and R_0 is a cutoff radius of 15 cm. The deposition shape is defined as $(E_{5\times5} - E_{3\times3})/E_{5\times5}$, where $E_{3\times3}$ and $E_{5\times5}$ are the deposited energies in 3×3 and 5×5 crystals around the cluster seed, respectively.

[38] M. Ablikim et al. (BESIII Collaboration), Phys. Rev. D **83**, 112005 (2011).

[39] L. Liu, X. Zhou, and H. Peng, Nucl. Instrum. Meth. A **1033**, 166672 (2022).

[40] B. Borasoy and B. R. Holstein, Phys. Rev. D **59**, 054019 (1999).

[41] G. R. Farrar, Phys. Rev. D **4**, 212 (1971).